

Electron Parallel Heat Transport in the Scrape-off Layer Using a Particle-in-Cell Code

Aaron FROESE, Tomonori TAKIZUKA¹⁾ and Masatoshi YAGI²⁾

IGSES, Kyushu University, Kasuga 816-8580, Japan

¹⁾*Japan Atomic Energy Agency, Naka 311-0193, Japan*

²⁾*RIAM, Kyushu University, Kasuga 816-8580, Japan*

(Received 14 January 2009 / Accepted 22 May 2009)

Electron heat transport parallel to the magnetic field in the scrape-off layer plasma is investigated with the use of the particle-in-cell code PARASOL. Coulomb collisions are simulated correctly by a binary collision model. The heat flux is lost by radiation cooling, in addition to convection/conduction to the divertor plates. It is confirmed for the collisional case that the conductive heat flux is given by the Spitzer-Härm expression. For the long mean free path case, the conductive heat flux is limited to a factor α_e of the free streaming value. It is found that α_e is small (~ 0.1 of the sheath-limited value) for the low radiation condition, but becomes large (~ 1.0) for the high radiation condition.

© 2010 The Japan Society of Plasma Science and Nuclear Fusion Research

Keywords: tokamak scrape-off layer, conductive heat flux, PIC simulation, PARASOL, collisionless flux limit

DOI: 10.1585/pfr.5.S1017

1. Introduction

The divertor design in a tokamak reactor produces a separatrix system with closed magnetic field lines surrounded by open field lines terminating at the divertor plates. The burning core plasma lies inside the separatrix and exhibits good containment, though a large amount of heat is lost by anomalous transport and ELMs across the separatrix to the scrape-off layer (SOL). The heat in the SOL is carried mainly by parallel transport along the open magnetic field lines to the divertor plates. Therefore, the SOL acts as a mediator between the hot core and the solid divertor plates.

Many features must be addressed in the SOL that are absent in the core; the plasma can no longer be assumed to be collisionless and strong parallel gradients develop in the plasma profiles that negatively affect the containment. In order to reduce the huge heat load on the plates, divertor simulation studies using fluid modelling are devoted to optimizing the divertor configuration and operation scenario. However, assumptions regarding kinetic effects, such as boundary conditions at the wall, heat conductivity, and plasma viscosity, are significant liabilities for the fluid model and are typically addressed by introducing primitive approximations [1, 2], which must be validated separately by full kinetic modelling. This can be accomplished by particle methods that suffer from large statistical errors or finite-difference methods that suffer from inefficient phase-space coverage. In this paper, electron heat transport parallel to the magnetic field in the SOL plasma is investigated

with the use of the particle-in-cell code PARASOL [3, 4] in which Coulomb collisions are simulated correctly by a binary collision model [5].

2. Parallel Heat Conduction

Parallel heat conduction by electrons is given by

$$q_e = \frac{m_e}{2} \int d\mathbf{v} \cdot V^2 V_{\parallel} f_e(\mathbf{x}, \mathbf{v}), \quad (1)$$

where m_e is the electron mass, \mathbf{v} is the particle velocity, $\mathbf{V} = \mathbf{v} - \mathbf{u}$ is the velocity relative to the fluid velocity \mathbf{u} , V_{\parallel} is the fluid velocity parallel to the magnetic field, and $f_e(\mathbf{x}, \mathbf{v})$ is the phase-space distribution function. In a collisional plasma, this leads to the Spitzer-Härm expression [6],

$$q_{\text{SH}} = -\kappa_e^{\text{SH}} \nabla_{\parallel} T_e \quad \kappa_e^{\text{SH}} = 3.2 n_e v_{te} \lambda_{ee}, \quad (2)$$

where κ_e^{SH} is the electron heat conductivity, n_e is the electron density, $v_{te} = (T_e/m_e)^{1/2}$ is the thermal speed, $T_e = n^{-1} \int d\mathbf{v} \cdot v^2 f_e(\mathbf{x}, \mathbf{v})$ is the electron temperature, $\lambda_{ee} = v_{te} \tau_{ee}$ is the thermal mean free path, and $\tau_{ee} \propto v_{te}^3$ is the electron-electron collision time. This expression is not general, since the proportional relationship with the mean free path would make the heat flux unbounded in a collisionless plasma. The maximum heat flux is the order of the one-way free-streaming flux

$$q_{\text{FS}} = n_e T_e (T_{e\parallel}/m_e)^{1/2}, \quad (3)$$

where $T_{e\parallel} = n^{-1} \int d\mathbf{v} \cdot v_{\parallel}^2 f_e(\mathbf{x}, \mathbf{v})$ is the parallel electron temperature. We wish to determine the collision-dependent behavior of the heat flux, so as to replace it with a simpler

author's e-mail: aaron@riam.kyushu-u.ac.jp

expression that retains reasonable accuracy. The preferred method is using the harmonic average form [1],

$$q_{\text{eff}} = \left(\frac{1}{q_{\text{SH}}} + \frac{1}{\alpha_e q_{\text{FS}}} \right)^{-1}, \quad \alpha_e \equiv \lim_{\lambda_{ee} \rightarrow \infty} \frac{q_e}{q_{\text{FS}}}, \quad (4)$$

where α_e is the flux-limiting coefficient, i.e. the ratio between free-streaming and actual heat fluxes in the collisionless limit. Since the Spitzer-Härm heat flux is proportional to the mean free path, when the collisionality is high, it becomes small, $q_{\text{SH}} \ll \alpha_e q_{\text{FS}}$, and $q_{\text{eff}} \approx q_{\text{SH}}$, but when the collisionality is low, it becomes large $q_{\text{SH}} \gg \alpha_e q_{\text{FS}}$ and $q_{\text{eff}} \approx \alpha_e q_{\text{FS}}$. A number of studies using kinetic simulations have produced widely disparate values for α_e , ranging from 0.03 to 3 [2]. However, there has been little inquiry into the cause of this range of results, with the exception of an investigation of the effect of collisionality using BIT1 [7]. In this study, we investigate the effects of collisionality, electron radiation rate, ion-electron mass ratio, and distance from the divertor plates on the electron conductive heat flux and heat flux limiter α_e .

3. Simulation Model

PARASOL is a electrostatic particle-in-cell model in a bounded domain with particle/energy sources and sinks. In this study, motion is in one-dimension and the domain is symmetric across the midpoint. Ions are fully traced (1d3v) while electrons follow their guiding centers (1d2v). A slab geometry is employed with plasma properties assumed to be homogenous in the directions perpendicular to the magnetic field. Both electrons and ions move in the spatial dimension s parallel to a magnetic field line with connection length L_{\parallel} lying on the separatrix. This is equivalent to a projection in the poloidal direction with particles moving along $x = \Theta s$ over length $L = \Theta L_{\parallel}$, where $\Theta = B_x/B$ is the ratio of the poloidal magnetic field to the total field strength. For simplicity, the magnetic field has been set to $\Theta = 0.2$.

The half-domain shown in Fig. 1 is divided into three major regions: source, intermediate, and radiation. A hot ambipolar plasma source is in the domain center $x/L = [0.4, 0.5]$ to model diffusion from the plasma core and a radiative energy sink lies beside the divertor $x/L =$

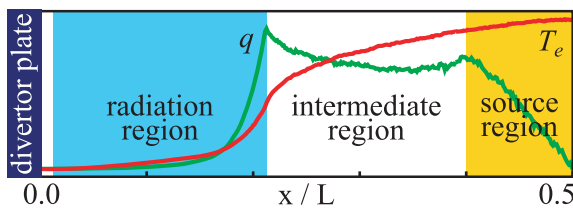


Fig. 1 Diagram of PARASOL half-domain showing the temperature and heat flux profiles in the system with $f_{\text{rad}} = 0.5$ and $\lambda_{\text{mfp}}/L = 0.1$. The divertor plate (navy) and radiation (blue), intermediate (white), and source (yellow) regions are marked.

[0.01, 0.21]. There is no source or sink behavior in the intermediate region $x/L = [0.21, 0.4]$. Particles generated at the source are given a thermal velocity distribution of isotropic temperature T_{e0} . All electrons occupying the radiation region lose a small fraction of their kinetic energy at each time step with no change in pitch angle. The input parameter $f_{\text{rad}} = Q_{\text{rad}}/Q_{\text{tot}}$ is the ratio between the radiative energy-loss flux to the energy flux entering the radiation region.

Divertor plates are located at the domain boundary $x = 0$. Besides the radiation loss, energy loss also occurs when particles reach the plate and are removed from the system. Ions that strike the divertor plate are reintroduced into the source region as a hot ion-electron pair, maintaining a constant ion number in the simulation. Due to the fact that electrons escape faster than ions, this leads to the existence of a sheath potential and a positive bias in the plasma. For this study, there is no recycling in the divertor region and neutrals are ignored for simplicity.

Coulomb collisions are treated using a binary collision model [5], where in each time step each particle is paired with both an ion and electron in the same cell and given a scattering angle. While the initial mean free path is specified as an input parameter

$$\lambda_{\text{mfp}0} \equiv 3^{3/2} \lambda_{ee} = \frac{6 \sqrt{3} \pi \varepsilon_0^2}{e^4 n_{e0} \Lambda} T_{e0}^2, \quad (5)$$

where ε_0 is the permittivity of free space, e is the elementary charge, Λ is the Coulomb logarithm, and the subscript '0' indicates an initial value. The actual mean free path evolves with the local plasma density and temperature such that $\lambda_{\text{mfp}}/\lambda_{\text{mfp}0} = n_{e0}/n_e (T_{e\parallel}/T_{e0})^{1/2} (T_e/T_{e0})^{3/2}$. The ion gyro-radius is set to $\rho_i/L = 5 \times 10^{-3}$, the number of spatial cells to 800, and the number of ions to $N_0 = 10^5$. Except where specified, the ion-electron mass ratio is $m_i/m_e = 1800$.

4. Results

One can see in Fig. 2 that different collisionalities and radiation rates produce strong changes in the spatial profile of the heat flux. The collisional cases (red and blue) exhibit large gradients in potential, density, and temperature compared to the collisionless cases (green and purple). They consequently have much smaller heat fluxes. As is expected, increasing the radiation causes the temperature and heat flux to drop precipitously before the divertor plate, but actually increases the rate of energy loss from the core plasma. In the collisional cases, the thermal energy is equally partitioned between all three dimensions, such that $T_{\parallel} = T_{\perp}$, whereas in the collisionless cases, the thermal energy is equally partitioned parallel and perpendicular to the magnetic field, such that $T_{\parallel} = T_{\perp}/2$.

The PARASOL code has previously been used to determine α_e to be a relatively high value of 0.75 for an ion electron mass ratio of $m_i/m_e = 400$ [3]. Figure 3 shows

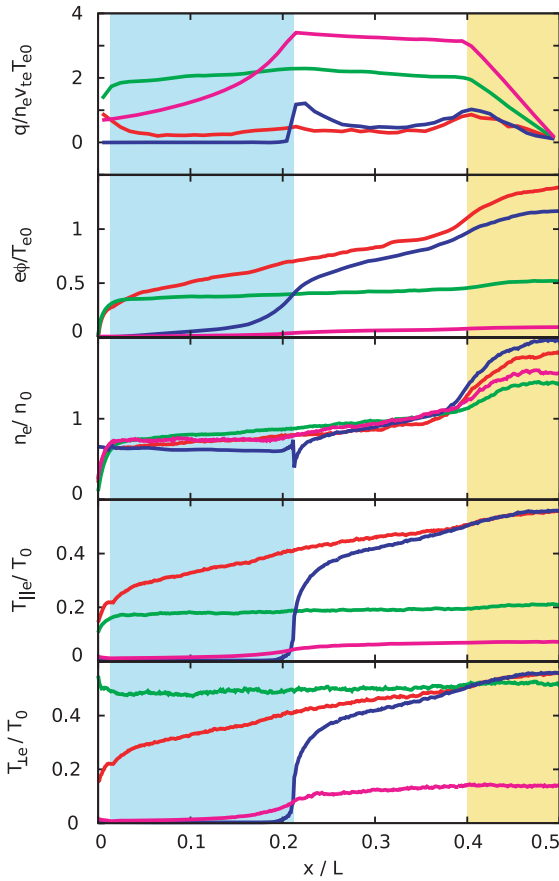


Fig. 2 Spatial variation profiles of conductive heat flux, potential, and electron density and temperature for plasma with the following properties: (red) low rad. $f_{\text{rad}} = 0.1$, collisional $\lambda_{\text{mfp}}/L = 10^{-2}$ (green) low rad. $f_{\text{rad}} = 0.1$, collisionless $\lambda_{\text{mfp}}/L = 10^2$ (blue) high rad. $f_{\text{rad}} = 0.5$, collisional $\lambda_{\text{mfp}}/L = 10^{-1}$ (purple) high rad. $f_{\text{rad}} = 0.5$, collisionless $\lambda_{\text{mfp}}/L = 10^3$

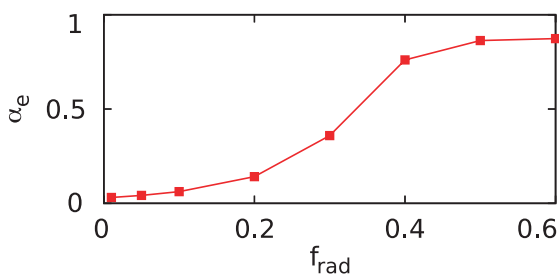


Fig. 3 Collisionless limit of the dependence of α_e on radiation rate f_{rad} .

that this falls within the range of possible values, when the radiation loss is large, $f_{\text{rad}} \sim 0.4$. The collisionless limit α_e has a simple harmonic form relationship with the radiation loss. As the radiation loss increases, α_e undergoes a transition from a small value to nearly unity. According to Fig. 4, this transition occurs at a higher radiation level as the mass ratio is increased. The mechanism by which α_e decreases as the mass ratio increases will be developed in

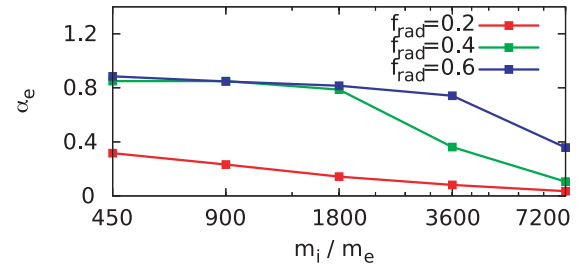


Fig. 4 Dependence of α_e in collisionless limit on ion-electron mass ratio m_i/m_e . Mass ratio 3600 corresponds to a deuterium plasma.

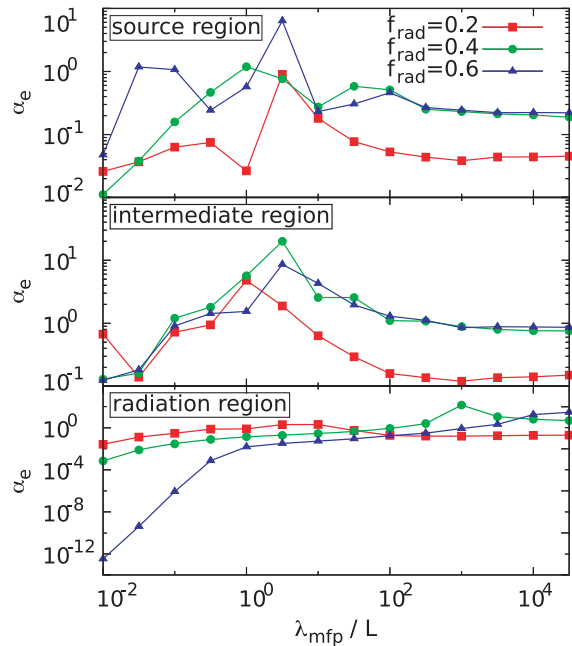


Fig. 5 Dependence of α_e on mean free path by region. Each point represents a poloidally-average over the indicated region with error bars omitted for clarity.

a forthcoming paper.

While α_e is defined as a collisionless limit without local energy sources or sinks, we wish to check if Eq. 4 can be used in the general case, as it often is. Therefore, the dependence of α_e on position and collisionality is of interest, with the results presented in Fig. 5. As expected, α_e always asymptotes to a constant value in the collisionless limit. This limit does not appear to depend on position (and hence, source and sink effects) much, in keeping with the expectation that a sheath-limited plasma is almost uniform. In contrast, source and sink effects strongly affect α_e in the collisional limit. In the source region, $q \approx q_{\text{SH}}$, which results in large errors in the calculated value of α_e . The intermediate region shows a radiation-independent nearly linear growth with $\alpha_e \propto \lambda_{\text{mfp}}$ that results in a peak when the mean free path is on the order of the connection length. The radiation region exhibits similar linear growth, except that high radiation produces a much more rapid increase in

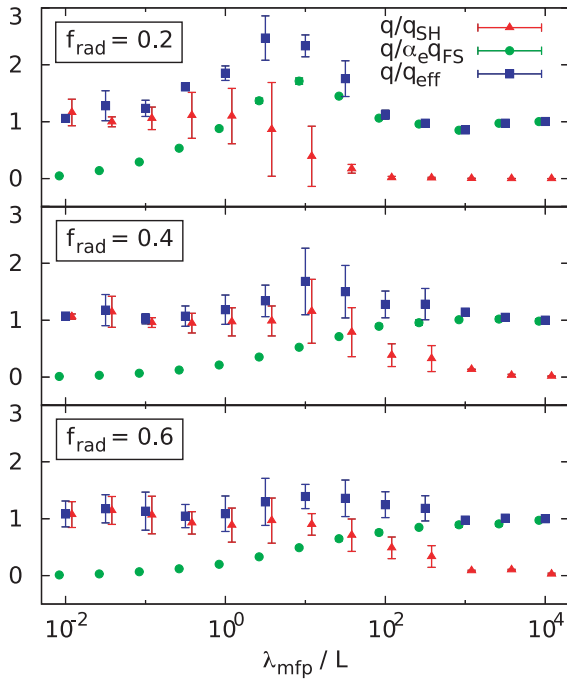


Fig. 6 Ratios of measured heat flux to Spitzer-Härm limit, α_e -adjusted free-streaming limit, and effective heat flux (Eq. 4) for different radiation rates and measured in the intermediate region. Error bars for $q/\alpha_e q_{FS}$ are too small to be visible. The values of α_e for each case are taken from the results in Fig. 6.

α_e than low radiation. The reason for this behavior will be investigated in the near future.

Further examining the validity of using q_{eff} in Eq. 4 as a general substitute for the heat flux that must otherwise be calculated by a fully kinetic simulation, Fig. 6 shows the relationship q/q_{eff} over a range of collisionalities and radiation rates. For comparison, the functions q/q_{eff} and $q/\alpha_e q_{FS}$ are also plotted. Of course, q/q_{eff} and $q/\alpha_e q_{FS}$ converge to unity at the collisionless limit because of the previous fitting to the free parameter α_e . However, without any fitting, the collisional limit also correctly shows that the heat flux approaches the Spitzer-Härm limit: $q \rightarrow q_{SH}$. Unfortunately, as the function transitions from the Spitzer-Härm limit to the free-streaming limit, the simple model deviates from the actual heat flux. When the radiation rate is high, the match between q_{eff} and q is acceptably within the error bars. However, at a moderate mean free path length of $1 < \lambda_{mfp}/L < 10$, a peak is evident such that the ratio q/q_{eff} is much larger than unity. This deviation of

the harmonic approximation q_{eff} from the actual heat flux q_e is currently under examination.

5. Summary

Electron heat transport parallel to the magnetic field in the SOL plasma is investigated with the PARASOL simulation. It is confirmed that in the collisional case the conductive heat flux is given by the Spitzer-Härm expression. In the collisionless case, conductive heat flux is limited to a factor α_e of the free-streaming value, which is small (~ 0.1 of the sheath-limited value) when little energy is lost to radiation, but becomes large (~ 1.0) when the radiation is high. Outside these limits, the currently used model of the conductive heat flux is an insufficient approximation for q_e . The model deviates strongly from the calculated results for a plasma with collisionality $1 < \lambda_{mfp}/L < 10$ and radiation less than $f_{rad} = 0.4$. Behavior in regions with energy sources or sinks also requires a multiply-defined α_e . Constraining usage of the model to regimes that behave correctly is not practical, and therefore, a more robust model is required. Due to the relative economy of system memory, a database lookup for q_e as a function of electron density and temperature may be the most tenable solution. Future work shall include investigation into the mechanism by which the heat flux becomes larger than the collisionless free-streaming limit, as well as the effects of other parameters, such as adjusting the width of the source and radiation regions.

Acknowledgments

We would like to thank Mr. M. Hosokawa for his collaboration with regards to the computation. We also thank Dr. D. Tskhakaya for his valuable input during our discussions. This work is partially supported by a JSPS Grant-in-Aid for Scientific Research (B) 19360415.

- [1] P.C. Stangeby, *The Plasma Boundary of Magnetic Fusion Devices* (Taylor & Francis, New York, 2000) p. 660.
- [2] W. Fundamenski, *Plasma Phys. Control. Fusion* **47**, R163 (2005).
- [3] T. Takizuka *et al.*, *Trans. Fusion Technol.* **39**, 111 (2001).
- [4] T. Takizuka, M. Hosokawa and K. Shimizu, *J. Nucl. Mater.* **290-293**, 753 (2001).
- [5] T. Takizuka and H. Abe, *J. Comput. Phys.* **25**, 205 (1977).
- [6] S.I. Braginskii, *Review of Plasma Physics Vol. 1*, edited by M. A. Leontovich (Consultants Bureau, New York, 1966) p. 205.
- [7] D. Tskhakaya *et al.*, *Contrib. Plasma Phys.* **48**, 89 (2008).